ChemCatChem 7 (2015) 3012-3019

DOI: 10.1002/cctc.201500355

Tuning the surface chemistry of nanoporous carbons for an enhanced nanoconfined photochemical activity

Leticia F. Velasco[a], Alicia Gomis-Berenguer[a], Joao C. Lima[b], Conchi O. Ania*[a]

Abstract: We showed the effect of surface oxidation on the conversion of light into chemical reaction in the confined pore space of nanoporous carbons. The photoactivity of carbons is due to the combination of high porosity and the presence of photoreactive sites that favor the splitting of the exciton inside the pores, hence boosting an efficient use in chemical reactions. The incorporation of O-groups in the carbon matrix decreased the photoconversion inside the pores, although values were higher than those attained in solution. This is attributed to the lower stabilization of the exciton through the delocalization within the conjugated sp^2 network of the basal planes, due to the withdrawal effect of the O-groups. The photochemical conversion of light inside the pores is very sensitive to the acidic/basic nature of the O-groups of the carbon matrix, and can be enhanced by balancing the surface composition, porosity, and electronic mobility.

Introduction

The conversion of light energy has been long explored in environmental chemistry for pollutants degradation, since the excitation of electronic molecular states may induce chemical bond breaking. Indeed, after the studies in 1977 reporting the performance of zinc and titanium oxides to decompose cyanides in solution,[1] the interest on the development of Advanced Oxidation Processes based on semiconductors photocatalysis for the degradation of pollutants in air and water has become very popular.[2]

Triggered by the low photonic efficiency of most semiconductors, optimizing the optical features of photoactive materials remains a largely investigated topic.[3] Aside from transition metal oxides and sulfides photocatalysts, hybrid materials prepared by their immobilization on appropriate substrates are being extensively investigated.[4] Despite carbons are strong light absorbing materials, their incorporation in hybrid carbon/semiconductor composites has been an interesting strategy to attain high photoconversion efficiencies in the degradation of a variety of pollutants.[5] First investigations in the field focused on the use of carbons as inert additives to TiO_2, and the enhanced performance of carbon/titania photocatalysts was attributed to i) the porosity of the inert porous carbon support, or ii) strong interfacial electronic effects in the case of carbon additives with high electronic mobility (i.e., carbon nanotubes, graphenes).[5]

Our recent research has demonstrated the photochemical activity of semiconductor-free nanoporous carbons under different irradiation conditions,[6] demonstrating their ability to photogenerate radical oxygen species (ROS) in aqueous environments.[7] This has opened new perspectives in the field of applied photochemistry based on carbon materials covering environmental remediation, water splitting, enhanced adsorption/oxidation, or photoluminescence.[8]

Despite the rising interest in the field, there is still a multitude of fundamental questions that are worth investigating to understand the underlying mechanisms governing the conversion of light into a chemical reaction leading to exploit the potential applications of light-responsive carbons in different fields.

Aiming at throwing some light on the topic, we herein provide an overview on the effect of the surface composition of nanoporous carbons on the photochemical reactions hosted inside the nanopores. By combining catalytic, spectroscopic and photoelectrochemical tools, we show the dependence of the photochemical response in the confined pore space with the surface functionalization of the carbon matrix, choosing the photooxidation of phenol as a model reaction.

Results and Discussion

Elucidating the mechanism of the photochemical reactions occurring in the constrained pore space of nanoporous solids is a complex task due to the simultaneous coexistence of various processes inherent to high energy irradiation sources and porous materials: direct and indirect photooxidation/reduction, reactions on the catalyst surface and adsorption and diffusion phenomena leading to changes in the reaction rate and reactants concentration. To disregard these contributions we have developed a strategy that allowed us to isolate and

[a] Dr. LF Velasco, A Gomis-Berenguer, Dr. CO Ania*
Instituto Nacional del Carbon (INCAR, CSIC)
C/Francisco Pintado Fe 26, 33011 Oviedo (Spain)
Fax: (+) 34 985297662
E-mail: conchi.ania@incar.csic.es

[b] Dr. JC Lima
Department of Chemistry, REQUIMTE/CQFB
Faculdade de Ciências e Tecnologia, Universidade Nova de Lisboa
2829-516 Lisboa, Portugal
Fax: (+):+351 2129544 61
E-mail: lima@dq.fct.unl.pt

Supporting information for this article is given via a link at the end of the document.

evaluate the efficiency of the photochemical reaction inside the pore voids of a catalyst.[6] The approach consisted in introducing a target compound inside its pore structure (adsorbed), before illuminating. After irradiation, the compounds still retained inside the porosity are extracted in an appropriate solvent and analyzed to determine the yield of the photochemical reaction that takes place inside the porosity of the material (Figure 1a). As no desorption occurs during the irradiation of the pre-adsorbed catalysts, the extent of the photochemical reaction provides direct evidence on the existence and fate of the host/light interactions in the confined pore space. Our previous studies have validated this experimental approach of monitoring the reaction from inside the pores for the photooxidation of phenol in aqueous solution using nanoporous carbons.[6]

Aiming at exploring the effect of the functionalization of the carbon matrix on the photochemical activity, we have prepared a series of oxidized materials by mild wet oxidation. It is important to highlight that the surface modification did not change the textural parameters of the pristine carbon (Table 1, see further characterization details in Figures S1-S5 in the Supporting Information) in terms of pore volume or surface area. This is most critical since the photochemical experiments were designed to control the amount adsorbed and the confinement state inside the porosity of the carbons.

Table 1. Main physicochemical and textural properties of the studied nanoporous carbons

Sample	B	BOH	BO
S_{BET} (m^2/g)	1033	1045	989
V_{total}[a] (cm^3/g)	0.52	0.52	0.50
V_{micro}[b] (cm^3/g)	0.32	0.32	0.31
V_{meso}[b] (cm^3/g)	0.09	0.08	0.07
pH_{PZC}	8.9	5.7	3.3
O wt.%[c]	2.1	6.4	7.5
CO (μmol/g)[d]	491	1903	1945
CO_2 (μmol/g)[d]	167	238	647

[a] Evaluated at a relative pressure 0.99. [b] Evaluated from DFT method. [c] On dry basis. [d] From TPD-MS measurements.

Also, according to literature[9] the incorporation of O-groups on nanoporous carbons decreases the uptake of phenol, although it does not alter the adsorption mechanism, which is governed by dispersive interactions between the pore walls and phenol molecules. To overcome these differences in the adsorption capacity upon oxidation, the amount of phenol preadsorbed before the irradiation was fixed and kept below their corresponding saturation limit. This allows to form a single adsorption layer in the pores (phenol molecules are predominantly adsorbed in an edge-wide orientation, with the aromatic ring parallel to the pore walls and the hydroxyl moiety projecting toward the solution),[9] and to assume that the confinement of phenol is the same for all the samples. Hence, the differences in the photochemical performance should be due to the nature and fate of the carbon/light interactions in the pore space.

Figure 1 shows the evolution of (b) phenol conversion and (c) intermediates detected in the extracts upon irradiation of the pre-adsorbed carbons using a low pressure Hg lamp. Data corresponding to direct photolysis (absence of catalyst) is also included for comparison. As seen, the three tested materials lead to very similar phenol conversion values. Furthermore, the superior photooxidation performance of the carbons over the photolytic reaction confirmed that the light conversion is boosted in the nanoconfined pore space. The effect is already very pronounced at short irradiation times, and for instance, after 150 min of irradiation the conversion of phenol is about 8 times higher inside the porous network of sample B than in the absence of catalyst. This is most remarkable considering that the carbon matrix absorbs a large fraction of the incident irradiation, for which the actual fraction of light responsible for the photochemical conversion of phenol inside the pores is expected to be much lower than in solution.

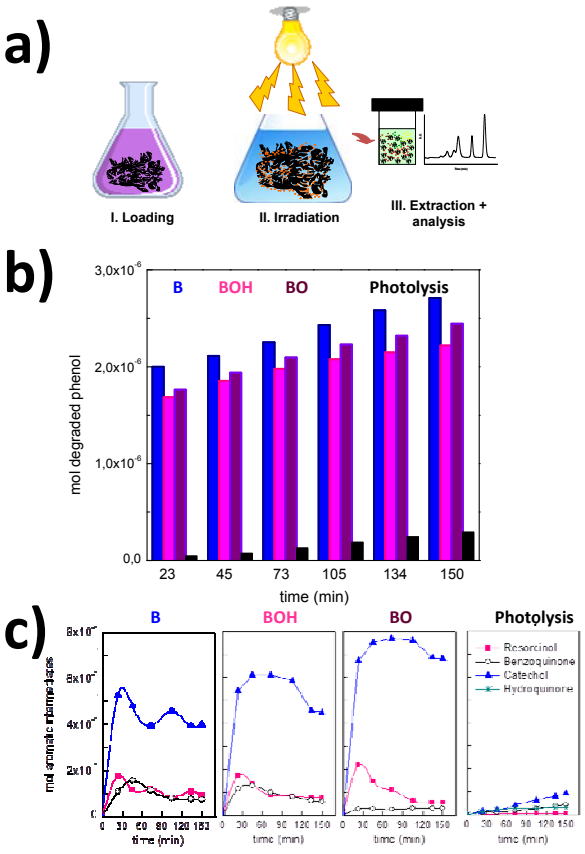

Figure 1. a) Scheme of the experimental procedure designed for evaluating the photochemical yield inside the nanopore structure of the carbon materials; b) phenol conversion and c) intermediates formed during the photocatalytic

reaction in the presence of activated carbons B, BOH and BO. Data corresponding to direct photolysis is also included for comparison purposes.

The amount of intermediates detected inside the nanopores is also larger than in solution (Figure 1c), which seems reasonable considering that phenol conversion is higher. It is interesting to point out that while for the carbons the amount of intermediates decreases with time, there is a clear accumulation of subproducts for the photolytic reaction. Another important difference can be seen in the speciation of the intermediates (Figure 1b); catechol is the predominant intermediate in all the cases, although its concentration is larger when phenol is decomposed inside the nanopore space. This finding is most significant given that the regioselective degradation of phenol in the ortho position is considered more advantageous than the conversion via the formation of quinones,[10] as the mechanism involves a lower number of intermediates. All this confirms that the non-catalyzed photodegradation is less efficient than the photooxidation inside the pores of the carbons.

As for the effect of surface chemistry, the better performance for the pristine carbon over the oxidized counterparts indicates the negative impact of the oxidation on the photochemical conversion of phenol. The abundance of degradation subproducts followed the trend: BO>BOH>B. This means that the incorporation of O-functionalities does not only reduce the conversion of phenol itself, but also the subsequent oxidation of the intermediates. Hence, the overall phenol photooxidation is more efficient on the parent carbon.

To gain further insight on the effect of the surface chemistry of the carbons in the photochemical conversion of light in the confined pore space, we calculated the photochemical quantum yield (ϕ) -defined by IUPAC as the ratio between the amount (mol) reacted, ΔN, per mol of photons absorbed ($I_A \Delta t$),[11]- from the slope of the correlation between the moles of degraded compounds per incident photon flux vs the irradiation time (Figure 2) with the equation:

$$\Delta N = \phi \, I_A \, \Delta t$$

where I_A is the photon flux absorbed by the sample, evaluated from the product of the incident photon flux I_o, determined by actinometry, and the integrated absorption fraction over the wavelength range used in the experiments (see details in the Supporting Information).

When the photochemical reaction occurs inside the nanopores it becomes very complex to evaluate the actual photon flux reaching the molecules adsorbed in the pores due to the contributions of light scattering by the particles suspended in solution and the strong light absorption by the carbon matrix itself. For the sake of comparison we calculated an apparent or pseudo-photochemical quantum yield (ϕ_{ps}) for the carbons by assuming that all emitted photons eventually reach the fraction adsorbed inside the porosity. Although this is a simplistic approximation, it allows a straightforward comparison of this family of nanoporous carbons as all the experiments were recorded under similar conditions (in terms of carbon matrix, catalyst loading and particle size). Besides, the actual photon flux would be smaller due to the above-mentioned side reactions consuming photons, hence even if ϕ_{ps} cannot be strictly considered a quantum yield, it accounts for the minimum limit of the actual quantum yield value. What is more important, it provides a more accurate viewpoint of the overall photochemical reaction occurring inside the porosity of the carbons, by considering the intermediates formed in the course of the reaction.

The dependence of the number of moles reacted per photon flux with the irradiation time are shown in Figure 2. The profile of direct photolysis in solution followed the expected linear pattern with the irradiation time, with a quantum yield of 12 mmol/Einstein, in agreement with values reported in the literature.[12]

Interesting features are revealed when the photochemical reaction is carried out inside the porosity of the carbons. As opposed to the non catalyzed reaction, the dependence of ϕ_{ps} with time shows two different regimes. Below 30 min of irradiation the amount of moles reacted is very high for the nanoporous carbons with ϕ_{ps} values close to unity; at longer times a second less steep linear region is observed and ϕ_{ps} values fall down by an order of magnitude (still they are larger than in solution). This indicates that the photochemical reaction inside the nanopores is very fast at short irradiation times, and gradually leads to steady conversion values over time.

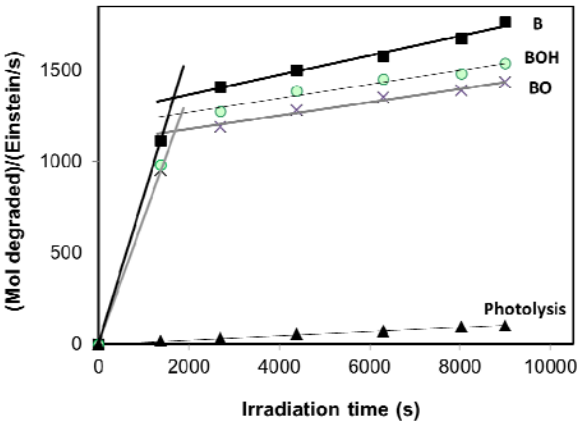

Figure 2. Correlation of the amount (mol) reacted per incident photon flux with the irradiation time for the nanoporous carbons and the photolytic reaction. Points represent experimental values, while lines are guides for the eye.

Regarding surface chemistry, ϕ_{ps} values followed the trend B>BOH>BO. Given the similar textural properties of the carbons (Table 1), differences in the photochemical response must be discussed in terms of the surface functionalization of the carbon matrix. Figure 3 shows the dependence of phenol conversion and ϕ_{ps} values with selected parameters of the nanoporous carbons characteristic of the degree of surface functionalization (oxygen content, surface pH, nature of O-groups). Data shows that the incorporation of oxygen groups of acidic nature is the most determinant parameter in the reduction of the photochemical activity. This is also supported by the correlations

with the amounts of gases (CO and CO_2) quantified from the thermodesorbed species by TPD-MS.

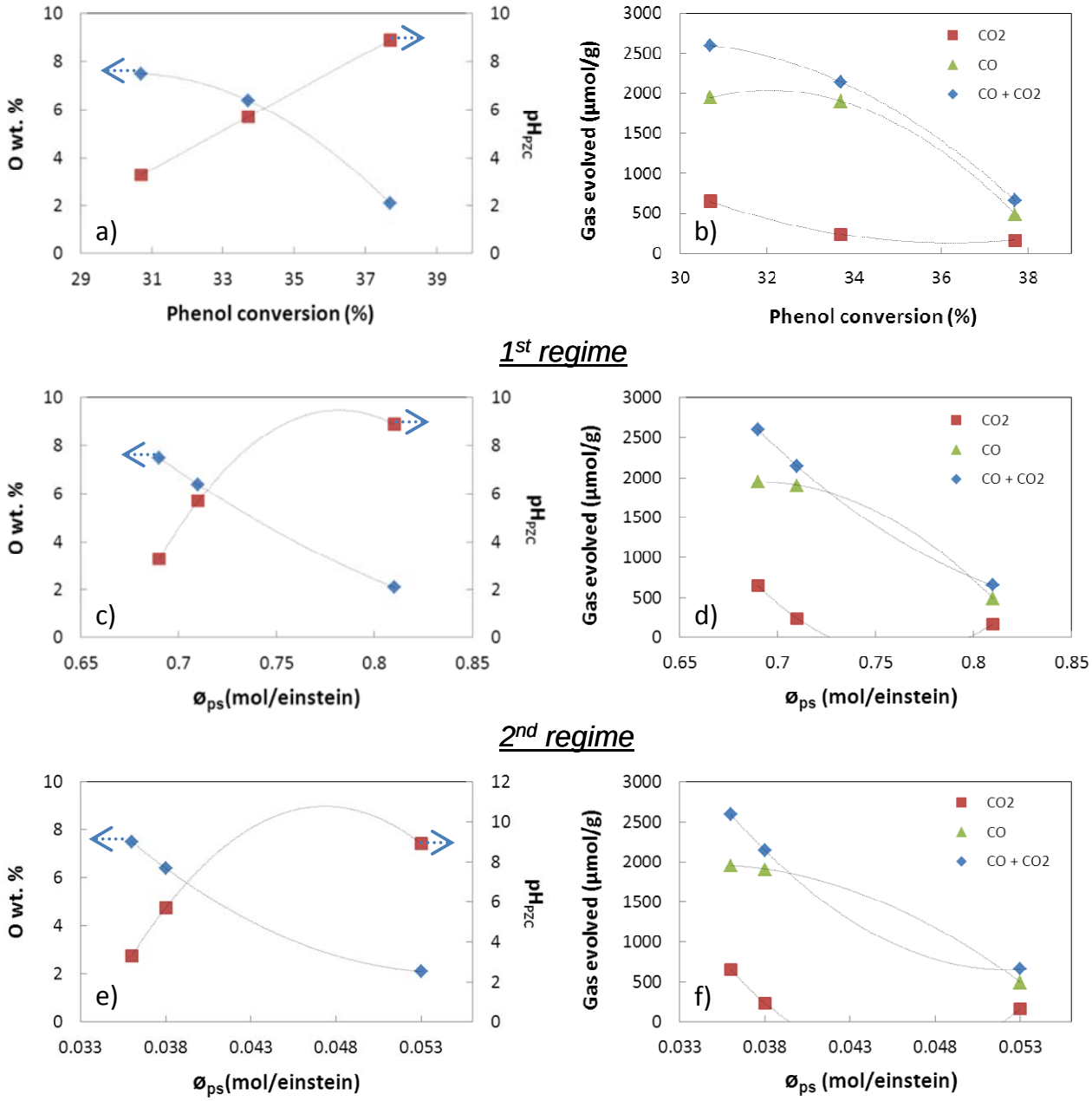

Figure 3. Effect of surface functionalization on phenol conversion (plots a-b) and ϕ_{ps} values (plots c-f) for the nanoporous carbons calculated for the first (plots c,d) and second (plots e,f) regime of the correlation of the moles reacted per incident photon flux with the irradiation time (see Figure 2).

As seen, the amount of CO_2-evolving groups (attributed to carboxylic acids and anhydrides of acidic nature) is about 3 times higher in BO than in BOH, whereas both carbons displayed quite similar amounts of CO-releasing groups (mainly phenolic and quinone-type groups).[13] Thus, the higher performance of BOH compared to BO is due to its increased surface hidrophobicity (Table 1, Figure 3). When data is analyzed considering the number of moles reacted (Figure 3c-f) and not just phenol conversion (Figure 3a-b), a similar trend is observed. In this case, the dependence with the chemical features of the carbons follows a polynomial pattern, indicating a

more sensitive response of the light conversion yield to small changes in the surface acidity of the nanoporous carbons.

According to literature, the light absorption features of amorphous nanoporous carbons depend on the density of electronic states, DOS, (mainly sp^2/sp^3 hybridization of the carbon atoms), and in the UV range are dominated by $\pi-\pi^*$ and $\sigma-\pi$ transitions involving free zig-zag sites and carbine-like sites.[14] Under sunlight irradiation, some other transitions involving the activation of chromophoric groups on the carbon surface have been proposed.[15] These electronic transitions generate carriers (holes and electrons), which if splitting is favored can participate in charge transfer reactions (either involving direct hole oxidation and/or radical mediated mechanisms) with electron donors present in the reaction medium.[14,15]

Considering this, the fall in the photochemical conversion in the functionalized carbons can be associated to several factors that would affect either their optical features (due to the creation of structural defects or changes in the sp^2/sp^3 hybridization state of carbon atoms derived from the incorporation of the O-groups) [6d,15] or the stabilization of the photogenerated carriers through the delocalization within the conjugated sp^2 network of the basal planes.

Several scenarios might be possible; the first one is that the holes might directly react with the adsorbed phenol molecules. This seems plausible as the reaction occurs inside the pores, and the splitting of the carriers would be favored by the immediate reaction with the adsorbed molecules. This explains the higher conversion values in the tight nanopore confinement compared to solution. However, since the carbons display similar textural features, it cannot account for the differences among the carbons themselves, which must be attributed to the fate of the charge carriers in the pores.

Another possibility is the stabilization of the holes through the oxidation of water molecules co-confined in the nanopore space, and the effect of the surface functionalization on the exciton splitting. This was supported by spin resonance spectroscopy (ESR) measurement that allowed the detection of radical species upon illumination of aqueous suspensions of the carbons, using a nitrone spin trapping agent (Figure 4).

For all the carbons similar ESR patterns were obtained, with the characteristic quartet peak profile with 1:2:2:1 intensity (g = 2.006, aN=abH=14.8 G hyperfine splitting constants), of the DMPO-OH adduct attributed to the presence of hydroxyl and superoxide radicals.[16] Quantification of the relative abundance of ROS showed lower concentration levels in the functionalized carbons. Interestingly, similar amounts of radicals were detected for carbons BO and BOH, pointing out the importance of the acidic/basic nature of the O-groups decorating the carbon surface (Table 1) in the formation of radicals. Indeed, the amount of ROS correlates well with the CO-evolving groups of basic nature (Figure S6), while the strong acidic groups (CO_2-evolving) seem to inhibit the formation of radicals. The high electron withdrawal effect of carboxylic acid and anhydride groups on the π-electron density of the carbon basal planes would increase the surface recombination of the carriers, thus resulting in lower radicals formation. Note that low ESR signals should not be considered as an indication of low photochemical activity; it only provides information about the formation of radicals, whereas the reaction may proceed via other mechanisms (e.g., direct hole transfer).[9] Thus, the lower ESR signals in the oxidized carbons indicate that the radical-mediated mechanism might not be the dominant mechanism.

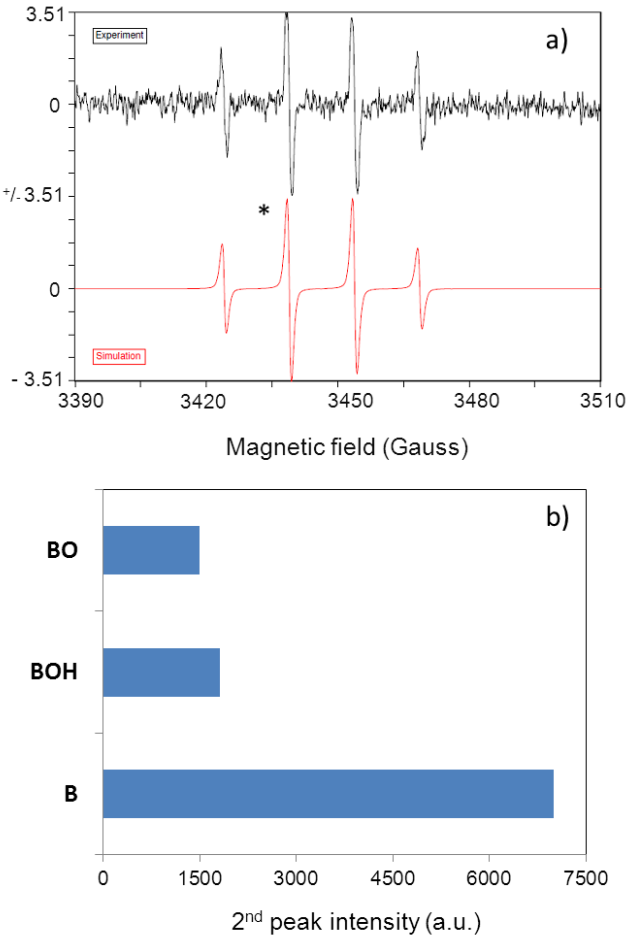

Figure 4. (a) Example of the ESR spectrum of the DMPO adducts obtained after 20 minutes of irradiation of aqueous suspensions of the nanoporous carbons; b) Quantification of the radical species corresponding to DMPO-OH adducts determined from the intensity of the second line (marked by a star) in the profiles.

Further insights into the fate of the photogenerated carriers were obtained by exploring the photoelectrochemical response of the carbons. Figure 5 shows the transient photocurrent response of the photoanodes after on/off illumination at various potentials. Dark currents at the applied potentials were allowed to equilibrate before the irradiation so as to stabilize the large capacitive contributions of the nanoporous carbon electrodes. The background photocurrent generated by illumination of the bare titanium foil used as current collector is also shown for comparison.

As seen, a remarkable photocurrent was generated when the electrodes were illuminated and the bias potential was positive enough for an efficient exciton separation. Furthermore, the potential onset of the photocurrent for the carbon anodes is about +0.8 V s Ag/AgCl, clearly lower than the value for the Ti collector.

The transient photocurrent response presents a square-shaped profile on switching-on the light (Figure 5b), with a prompt initial rise followed by smooth fall until a steady-state regime is achieved; the photocurrent retracts to original values once the illumination is turned off. In the aqueous electrolyte where water molecules are the only hole scavengers, the anodic photocurrent corresponds to water oxidation -corroborated by measuring the O_2 concentration in the electrolyte-, while the photogenerated electrons migrate to the substrate through the electrode film. The photocurrent response was stable and reproducible during repeated on/off cycles of illumination.

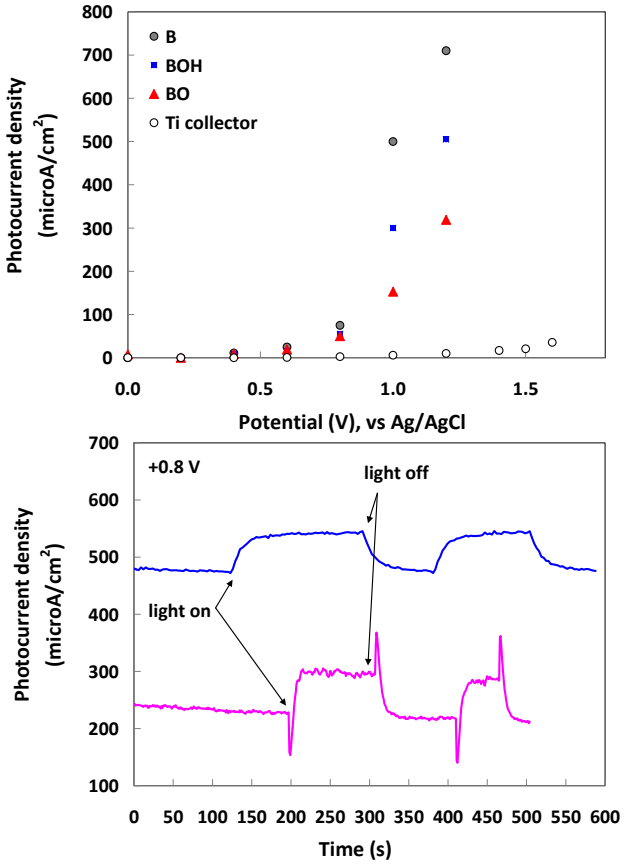

Figure 5. (a) Transient photocurrent densities vs bias potential of the nanoporous carbons; (b) example of the chronoamperometric response of photoelectrodes built on carbon B showing the square-shaped profile and the cathodic/anodic shoots in the transient photocurrent response.

In some electrodes the initial anodic rise upon illumination was preceded by a cathodic undershoot (Figure 5b), while the steady-state regime was followed by an anodic overshoot when the illumination was turned off. Anodic and cathodic current shoots are frequently reported for semiconductor materials and attributed to surface recombination processes of the photogenerated charges or photocorrosion phenomena.[17] In our materials the cathodic undershoot is most likely attributed to either the reduction of trace amounts of dissolved O_2 remaining in the pores of the carbons that could not be removed by N_2 bubbling (photocurrent disappears in subsequent cycles), and/or the reduction of photogenerated •OH radicals (according to the reaction •OH + 1 e- ↔ OH-), as evidenced by the ESR spectra (Figure 4).

The presence of undershoots can be used as an indicator for insufficient mass transport and poor efficient reaction. This is rather expected considering the low electron mobility of the studied nanoporous carbons (DC conductivity of ca. 0.5, 0.2 and 0.02 mS/cm for BO, BOH and BO, respectively).

At 1 V and above, the photocurrent density increased considerable for all the carbons due to the more efficient photoassisted oxygen evolution reaction when higher potential values are applied (extensive bubbling was seen on the electrode surface, not observed in dark or during irradiation of the bare collector).

All the carbons showed the same potential onset for the photocurrent detection, although current densities decreased for the functionalized materials. This contrasts with our previous work reporting the photoelectrochemical oxidation of water using visible light and highly functionalized carbon photoanodes.[15] The ability to oxidize water was linked to the presence of S- and N- groups working as chromophores, which upon light excitation leave reactive vacancies that are able to accept electrons from oxygen in water molecules. The role of sulfur and nitrogen species was supported by the lack of activity detected on a commercial nanoporous carbon free of these heteroatoms.

The fact that herein studied nanoporous carbons do not have S- and N- groups but display photochemical activity renders a new perspective on the origin of this behavior and on the role of surface chemistry. First of all, the porosity of these nanoporous carbons is more developed than that of the previously studied ones (Table 1, Figures S3 and S4), with larger pore volumes adapted for the adsorption of water and phenol (via dispersive forces).[9,18] Besides porosity, hydrogen bonding with the surface groups existing in the pores could be expected to promote the surface wetting and hence increasing the photoelectrochemical oxidation of water inside the pores. On the contrary, oxidation caused a reduced hydrophobicity of the carbons (Table 1). It seems that beyond surface wetting, the carbon materials must have photoactive sites inside the pores where carbon/light/water and/or carbon/light/phenol interactions can take place.

Certainly the photoactivity of these carbons is not linked to the presence of chromophoric surface groups -our previous studies also disregarded the contribution of metal impurities-,[7] but to the generation of carriers in the reactive sites. Such reactive sites in carbons are located at the edges of the basal planes, either associated to surface functionalities, or to free edges sites linked to various configurations (carbyne-like and carbene type).[19] The free sites are also responsible for the

reactivity of carbons to incorporate heteroatoms giving rise to stable surface functionalities).[19] Considering this, the reduced photoactivity of the oxidized carbons would be linked to a lower density of free reactive sites (where the O-groups are most likely incorporated).

Additionally, owing to the presence of O-groups and their high electron withdrawal on the π-electron density of the basal planes, oxidation of the carbons affects the stabilization/splitting of the exciton via the charge propagation through the carbon matrix, resulting in higher surface recombination (i.e., lower photocurrents). Further support for the superior electron mobility in the pristine carbon is in its highest DC conductivity.

The stability of the carbon photoanodes after the on/off illumination cycles was also explored; the materials proved to be quite resistant to illumination (Figures S7, S8), but got oxidized when the bias potential was higher than 0.8 V vs Ag/AgCl due to the effect of the oxygen released during water oxidation. The TPD-MS analysis of the used photoanodes evidenced the oxidation and decrease in surface hybrophobicity, while the appearance of new humps in the cyclic voltammograms showed the loss of conductivity caused by these changes in the surface chemistry.

Finally it should be highlighted that current densities up to 0.70 mA/cm^2 were recorded for the highest potentials on sample B. Despite these are low values compared to data in the literature for the photoelectrochemical splitting of water,[20] they are most remarkable considering the nature of the carbon photoanodes (metal-free and amorphous nanoporous carbons) and the low overpotential for the photoelectrochemical oxidation of water.

Conclusions

Our results show that the conversion of light inside the porous network of nanoporous carbons depends on the porosity, surface functionalization and presence of photoreactive sites that lead to the photogeneration of charge carriers that can be effectively used in chemical reactions. The presence of a well developed porosity is essential to obtain high conversion in the constrained pore space, distinguishing low cost nanoporous carbons from graphene, carbon nanotubes or other nanostructured carbon materials.

Regarding functionalization, the decoration of the carbon surface with O-groups caused a decrease in the photooxidation of phenol inside the pores; however conversions were still higher in the confined pore space of the functionalized carbons than in solution.

Besides the density of surface groups, the yield of the light conversion is very sensitive to small changes on the acidic/basic strength of the oxygen groups, particularly to the presence of acidic ones (CO_2-releasing groups). The number of moles reacted increased with the surface hydrophobicity, as inferred by the superior performance of the carbons showing either low functionalization or mainly phenolic and quinone-type groups. This behavior is linked to the lower ability of the acidic carbons to stabilize/promote the splitting of the photogenerated exciton through the delocalization within the conjugated sp^2 network of the basal planes, due to the high withdrawal effect of O-donating groups. This was corroborated by the lower amount of oxygen radical species and lower photocurrent densities measured in the functionalized carbons.

Owing to the versatility of nanoporous carbons and abundance of precursors (allowing simple and cost effective synthetic methods), it is highly feasible to push the nanoporous carbons as sustainable metal-free photoanodes/cathode materials for different applications (e.g. photoelectrochemical water splitting for hydrogen and oxygen evolution, pollutants photooxidation). The future challenge is in further enhancing the photochemical activity by balancing the surface composition (via incorporating adequate photosensitizer groups), porosity, reactivity, and change-carrier mobility (increasing conductive graphene-like units). Work focused on optimizing the nanoporous carbon layout in a controlled way to achieve stable carbon photoelectrodes with higher efficiency is ongoing.

Experimental Section

Materials. A nanoporous carbon obtained from CO_2 activation of bituminous coal was selected for this study (sample B). The pristine carbon was submitted to several treatments to modify its composition aiming at exploring the effect of the surface chemistry on the photochemical response. The incorporation of oxygen was carried out by mild wet oxidation. About 1 g of sample was put in contact with 10 mL of a saturated solution of ammonium persulfate in 4 N H_2SO_4 at room temperature and left stirring overnight. After oxidation, the carbon was filtered out, washed with distilled water until constant pH and dried at 110 °C overnight (sample BO). Subsequently, an aliquot of this carbon was submitted to a thermal treatment at 400 °C during 30 minutes in a flow of nitrogen (50 mL/min) in order to partially remove the incorporated functionalities (sample BOH).

Characterization. The textural properties of the samples were determined by means of N_2 adsorption at -196 °C (Micromeritics, ASAP 2010). Before the experiments, samples were outgassed at 120 °C overnight to constant vacuum (10^{-4} Torr). The main textural parameters such as specific surface area, S_{BET}, pore volumes and distribution of pore sizes were evaluated from the nitrogen adsorption isotherms. The carbon materials were further characterized by elemental analysis (LECO CHNS-932 and LECO VTF-900 automatic analyzers). A custom made device for TPD-MS was also used to evaluate the surface chemistry of the activated carbons. The samples were heated in a silica fused reactor up to 900 °C at a heating rate of 10 °C min^{-1}. The analysis was done under high vacuum conditions (below 10^{-5} mbar) and the gas phase was continuously monitored by a mass spectrometer. The acidic/basic character of the nanoporous carbons was determined by the measurement of the pH of point of zero charge (pH_{PZC}) using a modification of the mass-titration method by Noh and Schwarz.[21]

Phenol photooxidation. A low pressure mercury lamp (6 W, emitting at 250, 401, 433 and 542 nm) was used as irradiation source. The incident photon flux of the lamp (ca.

3.3×10^{-9} Einstein s^{-1}) was measured through ferrioxalate actinometry[11] and used to normalize the photochemical conversions. Suspensions of the carbons in a phenol solution are allowed to equilibrate until all phenol is completely removed and then irradiated at different times. The solution is filtered out and analyzed by reverse phase HPLC (C18 column, water/methanol 95:5). The carbons are further extracted with ethanol and the alcoholic solution is also analyzed by HPLC. Extraction yields are previously determined for each pure compound on each carbon material. The corresponding blank of direct phenol photolysis was also performed under similar conditions for comparison. All the measurements were done at least in duplicates (standard deviation was lower than 5 %) and average values are presented.

Photoelectrochemical measurements. A standard three-electrode cell provided with an optically flat quartz window on the side, and consisting of the nanoporous carbon photoanode as a working electrode, a graphite rod as counter electrode, and a saturated Ag/AgCl reference electrode was used. For the preparation of the electrodes a slurry of the nanoporous carbon and PVDF (ratio 90:10) in N-methyl-2-pyrrolidone was coated on a 1 cm^2 Ti foil collector, and dried at 120 °C before usage. A Xe lamp emitting between 200-600 nm (150 W) was used as irradiation source to amplify the signal of the carbon electrodes. A potentiostat (Biologic) was used to evaluate the electrochemical behavior. The transient photocurrents were obtained under a constant bias potential between 0 and +1.5 V vs. Ag/AgCl under on/off illumination. Dark current equilibrium at the applied potential was allowed before the irradiation. The photoanodes were suspended in 20 mL of an aqueous solution of 0.1 M Na_2SO_4 and purged with N_2 before the illumination (dissolved O_2 concentration in the electrolyte was measured using a sensor). The electrochemical behavior of the electrodes was also explored by cyclic voltammetry at a potential sweep of 20 mV/s, before and after light exposure.

Spin Trapping Electron Spin Resonance (ESR) Measurements. The formation of paramagnetic species in solution during irradiation of the carbon suspensions was detected by a nitrone spin trapping agent (5,5-dimethylpyrroline-N-oxide, DMPO). This compound is capable of forming spin adducts with hydroxyl and superoxide radicals, creating more stable nitrone radicals that are easily detected by ESR spectroscopy in aqueous solution. About 0.5 g/L of the carbon samples were suspended in 5 mL of $HClO_4$ buffer (pH 3), and the appropriate volume of DMPO was added to the suspension to reach a final concentration of 18 mM. Samples were introduced in capillary quartz tubes and irradiated for 5, 10, 20 and 60 minutes (Philips TL K40W/05 lamp, with a broad emission peak centered at 365 nm). ESR spectra were immediately recorded from the solution (after filtering out the solids) at room temperature on a Bruker ESP 300E X band spectrometer with the following spectral parameters: receiver gain 10^5; modulation amplitude 0.52 G; modulation frequency 100 kHz, microwave frequency 9.69 GHz; microwave power 5.024 mW; conversion time 40.96 ms; center field 3450 G, sweep width 120 G. The intensity of the second line in the spectra was used for the quantification of the signals.

Acknowledgements

The financial support of the Spanish MINECO (grant CTM2014-56770-R) is acknowledged.

Keywords: photochemistry • nanoporous carbons • surface chemistry • nanoconfined photochemical reactions

[1] a) T. I. Barry, F. S. Stone, *Proc. Royal Soc.* **1960**, *255*, 124-144; b) F. Romero-Rossi, F. S. Stone, *2nd Intern. Congr. on Catalysis*, Paris, **1960**, 1481-1497; c) R. I. Bickley, G. Munuera, F. S. Stone, *J. Catal.* **1973**, *31*, 398-407; d) A. Fujishima, K. Honda, *Nature* **1972**, *238*, 37-38.

[2] a) D.F. Ollis, DH. Al-Ekabi. H. in Photocatalytic purification and treatment of water and air, Elsevier, 1993; b) E Pelizzetti, N Serpone, in Photocatalysis: fundamentals and applications. New York, Wiley, 1989; c) M. A. Henderson, *Surf. Sci. Rep.* **2011**, *66*, 185-297; d) M. Kaneko, I. Okura, in Photocatalysis: science and technology, Springer, **2002**; e) M. R. Hoffmann, S. T. Martin, W. Choi, D. W. Bahnemann, *Chem. Rev.* **1995**, 95, 69-96.

[3] a) S. Das, W.M.A. Wan Daud, Renew. Sust. Energ. Rev. 2014, 39, 765-805; b) H. Kisch, Angew. Chem. Int. 2013, 52(3), 812-847; c) X. Zong, L. Wang, J. Photoch. Photobio. C 2014, 18, 32-49; d) G. Colón, S. Murcia-López, M.C. Hidalgo, J.A. Navío, *Chem. Commun.* **2010**, 46, 4809-4811; e) J.G. Yu, J.F Xiong, B. Cheng, Y. Yu, J.B. Wang, *J. Solid State Chem* **2005**, 178, 1968-1972

[4] a) H Choi, E. Stathatos, D. Dionysiou, Appl. Catal. B, **2006**, 63, 60-67; b) L. Erdeia, N. Arecrachakula, S. Vigneswaran, *Sep. Purif. Technol.,* 2008, 62, 382-388; c) A. Fernández, G. Lassaletta, V. M. Jiménez, A. Justo, A. R. González-Elipe, J. M. Herrmann, H. Tahiri, Y. Ait-Ichou, Y. *Appl. Catal. B Environ.* **1995**, 7, 49-63.

[5] a) J. Matos, J. Laine, J. M. Herrmann, *Appl. Catal. B Environ.,* **1998**, 8, 281-291; b) G. L. Puma, A. Bono, D. Krishnaiah, J. G. Collin, *J. Hazard. Mater.* 2008, 157, 209-19; c) B. Tryba, A. W. Morawski, M. Inagaki, *Appl Catal B,* **2003**, 41, 427-33; d) R. Leary, A. Westwood, *Carbon* **2011**, *49*, 741-772; e) J. L. Faria, W. Wang, in *Carbon materials for catalysis*, Chapter 13 (Eds.: P. Serp, J. L. Figueiredo), John Wiley & Sons, New York, **2009**, pp. 481-506;

[6] a) L. F. Velasco, I. M. Fonseca, J. B. Parra, J. C. Lima, C. O. Ania, *Carbon* **2012**, *50*, 249-258; b) L. F. Velasco, J. B. Parra, C. O. Ania, *Appl. Surf. Sci.* **2010**, *256*, 5254-5258. c) C. O. Ania, L. F. Velasco, T. Valdes-Solis, in *Novel Carbon Adsorbents*, Chapter 17 (Ed: J. M. D. Tascon), Elsevier, London, **2012** pp. 521-547; d) L.F. Velasco, J.C. Lima and C.O. Ania, *Angew. Chem. Int. Ed*., **2014**, 53, 4146-4148.

[7] a) L. F. Velasco, V. Maurino, E. Laurenti, I. M. Fonseca, J. C. Lima, C. O. Ania, *Appl. Catal. A* **2013**, *452*, 1-8; b) L. F. Velasco, V. Maurino, E. Laurenti, C. O. Ania, *Appl. Catal. A* **2013**, *453*, 310-315.

[8] a) L. Bao, Z.L. Zhang, Z.Q. Tian, L. Zhang, C. Liu, Y. Lin, B. Qi and D.W. Pang, *Adv. Mater.*, **2011**, 23, 5801; b) Q. Bao, J. Zhang, C. Pan, J. Li, C.M. Li, J. Zang, D.Y. Tang, *J. Phys. Chem. C,* **2007**, 111, 10347; c) T.J. Bandosz, E. Rodriguez-Castellon, J.M. Montenegro, M. Seredych, *Carbon*, **2014**, 77, 651; d) M. Seredych, O. Mabayoje, T.J. Bandosz, *Langmuir*, **2012**, 28, 1337; e) D. Pan, J. Zhang, Z. Li, M. Wu, *Adv. Mater.,* **2010**, 22, 734; f) I. Velo-Gala, J.J. Lopez-Peñalver, M. Sanchez-Polo, J. Ribera-Utrilla, *Appl. Catal. B,* **2013**, 142, 694; g) T. J. Bandosz, J. Matos, Seredych, M. S. Z. Islam, R. Alfano, *Appl. Catal. A* **2012**, *445*, 159-165; h) R. Ocampo-Pérez, M. Sánchez-Polo, J. Rivera-Utrilla, R. Leyva-Ramos, *Appl. Catal. B Envir*., **2011**, 104, 177.

[9] a) L.F. Velasco and C.O. Ania, *Adsorption*, 2011, **17**, 247; b) L.R. Radovic, C. Moreno-Castilla, J. Rivera-Utrilla in Chemistry and Physics

of Carbon (Ed. L.R. Radovic), New York: Marcel Dekker**, 2000**, pp. 227-405; c) D.D. Singh, *Ind. J. Chem.*, **1971**, 9, 1369.

[10] A. Santos, P. Yustos, A. Quintanilla, S. Rodríguez, F. Garcia-Ochoa, *Appl. Catal. B: Environ*. **2002**, 39, 97-113

[11] a) H. K. Kuhn, S. E. Braslavsky, R. Schmidt, *Pure Appl. Chem.* **2004**, *76*, 2105-2146; b) S.E. Braslavsky, *Pure App. Chem.,* **2007**, 79, 293-465.

[12] a) O. Gimeno, M. Carbajo , F. J., Beltran, F. J. Rivas, *J Hazard Mater* **2005**, 119, 99-108; b) M. Rodrıguez, A. B. Abderrazik, S. Contreras, E. Chamarro, J. Gimenez, S. Esplugas, *Appl Catal B* **2002**, 37, 131-7; c) H. Kusic, N. Koprivanac, A. L. Bozic, I. Selanec, *J Hazard Mater* **2006**, 136, 632-44.

[13] a) J. L. Figueiredo, M. F. R. Pereira, M. M. A. Freitas, J. J. M. Orfao, *Carbon* **1999**, 37, 1379–1389; b) T.J. Bandosz, C.O. Ania,. in Surface chemistry of activated carbons and its characterization. (ed. T.J. Bandosz) Activated Carbon Surfaces in Environmental Remediation. Interface Science and Technology, Elsevier, New York, **2006,** pp. 159–229.

[14] a) A. D. Modestov, J. Gun, O. Lev, *Surf. Sci.* **1998**, *417*, 311-322; b) A. D. Modestov, J. Gun, O. Lev, *J. Electroanal. Chem.* **1999**, *476*, 118-131; c) J. Robertson, *J. Phys. Rev. Lett* **1992**, *68*, 220-223; d) C. Oppedisano, A. Tagliaferro, *Appl. Phys. Lett* **1999**, *75*, 3650-3652; e) J. Robertson, *Mat. Sci. Eng. R Reports* **2002**, *37*, 129-281; f) L.R. Radovic and B. Bockrath, *J. Am. Chem. Soc.*, 2005, **127**, 5917; g) Y. Zhao, R. Nakamura, K. Kamiya, S. Nakanishi and K. Hashimoto, *Nature Comm.*, 2013, **4**, 2390; h) I. Velo-Gala, J. J. Lopez-Peñalver, M. Sanchez-Polo, J. Ribera-Utrilla, *Appl. Catal. B Environ.* **2013**, *142-143*, 694-704.

[15] C.O. Ania, M. Seredych, E. Rodriguez-Castellon, T.J. Bandosz, *Carbon*, **2014**, 79, 432

[16] a) E. Finkelstein, G. M. Rose, E. J. Rauckman, J. Paxton, *J. Mol. Pharmacol*. **1979**, 16, 676-685; b) B. Gray, A. J. Carmichael, *Biochem. J.* **1992**, 281, 795-802

[17] a) J. Ronge, D. Nijs, S. Kerkhofs, K. Masschaele, J. A. Martens, *Phys. Chem. Chem. Phys.,* **2013**, 15, 9315; b) L. M. Peter, *Chem Rev* **1990**, 90, 753-769; c) M. C. Long, R. Beranek, W. M. Cai, H. Kisch, *Electrochim Acta* **2008**, 53, 4621-4626.

[18] J.K. Brennan, T.J. Bandosz, K. T. Thomson, K. E. Gubbins, *Colloids Surf A: Physicochem Eng Asp,* **2001**, 187-188, 539-68.

[19] a) L. R. Radovic, P.L. Walker, R. G. Jenkins, *Fuel*, **1983**, 62, 849-856; b) L. R. Radovic, B. Bockrath, *J. Am. Chem. Soc.,* **2005**, 127, 5917-5927; c) L. R. Radovic, A. F. Silva-Villalobos, A. B. Silva-Tapia, F. Vallejos-Burgos, *Carbon* **2011**, 49, 3471-3487.

[20] a) D. Wang, T. Hisatomi, T, Takata, C. Pan, M. Katayama, J. Kubota, K. Domen, *Angew Chem Int Ed* **2013**, 52, 11252-6; b) K. Maeda, D. Lu, K. Domen, *Chem Eur J* **2013**, 19, 4986-91; c) K, Maeda, *Chem Commun* **2013**, 49, 8404-6; d) G. Xie, K. Zhang, B. Guo, Q. Liu, L. Fang, J. R. Gong, Adv Mater., 2013, 25, 3820-39; e) Y. K. Kim, H. Park, *Appl. Catal. B Environ.,* **2012**, 125, 530-7.

[21] J. S. Noh, J. A. Schwarz, *J. Colloid Interface Sci.* **1989**, 130, 157-164.

Supporting Information

Characterization of the nanoporous carbons

Thermal analysis-mass spectrometry (TA-MS): Thermal analysis was carried out using a thermogravimetric analyzer from Setaram. Experiments were carried out under an argon flow rate of 50 cm^3 min^{-1}, at a heating rate of 10 ºC min^{-1}, up to a final temperature of 900 °C. For each experiment, about 25 mg of a carbon sample was used. Temperature programmed desorption (TPD) experiments to evaluate the surface chemistry were also carried out in a custom made device. The samples were heated in a silica fused reactor up to 900 °C at a heating rate of 10 °C min^{-1}. The analysis was done under high vacuum conditions (below 10^{-5} mbar) and the gas phase was continuously monitored by a mass spectrometer. The amount of CO and CO_2 evolved during the TPD experiments were quantified.

DC Conductivity measurements: The DC conductivity was measured using a 4-probe method on the disk-shaped pellets (diameter 9 mm) with the composition 90 wt. % of carbon material and 10 wt. % PVDF as binder. The measurement of conductivity was carried out using the Keithley 2400 multimeter using the van der Pauw technique [van der Pauw J. A Method of Measuring Specific Resistivity and Hall Effect of Discs of Arbitrary Shapes. Philips Res Repts, 1958;13:1–9.28], which involves the application of a bias current of 50 mA to the carbon pellets and measuring the voltage drop, using a four probe configuration.

*Potentiometric Titration:T*he surface chemistry was characterized by the determination of the surface pH and proton binding curves by potentiometric titration. Briefly, subsamples of the initial materials (~ 0.125 g) were added to $NaNO_3$ (10mM, 50 mL) and equilibrated under stirring overnight. The suspensions are acidified in 0.1M HCl until pH 3 and titrated with 0.1 M NaOH up to pH 11 using an automatic analyzer. During the titration the suspension was purged with N_2 to eliminate the influence of atmospheric CO_2. The experimental data was transformed into proton binding curves, $Q(H^+)$, representing the total amount of protonated sites [20]. The crossover point with the pH axis on the titration curves, is the point where anion and cation exchange are in equilibrium (surface pH).

Chemical Actinometry and Quantum Yield

The photon flux of the irradiation sources was measured through ferrioxalate actinometry following IUPAC recommendations [H. K. Kuhn, S. E. Braslavsky, R. Schmidt, Pure Appl. Chem. 2004, 76, 2105-2146; S.E. Braslavsky, Pure App. Chem., 2007, 79, 293-465.7]. The quantum yield of phenol photolysis (ϕ) -defined as the ratio between the number of mol reacted, ΔN, and the mole of photons absorbed (IAΔt)- was evaluated from the slope of the relation between the mol of pollutant degraded vs the irradiation time, using the equation:

$$\Delta N = \phi I_A \Delta t$$

where IA is the photon flux absorbed by the sample, evaluated from the product of the incident photon flux Io, determined by actinometry, and the integrated absorption fraction FS over the wavelength range used in the experiment:

$$I_A = I_0 Fs = I_0 \left(1 - 10^{-\bar{A}_T}\right) \frac{\varepsilon_f \bar{C}_f b}{\bar{A}_T} \Delta t$$

being A_T the total absorbance given by the compound and its degradation intermediates, εf phenol molar absortivity coefficient, C_f the concentration of phenol, and b the light path in cm.

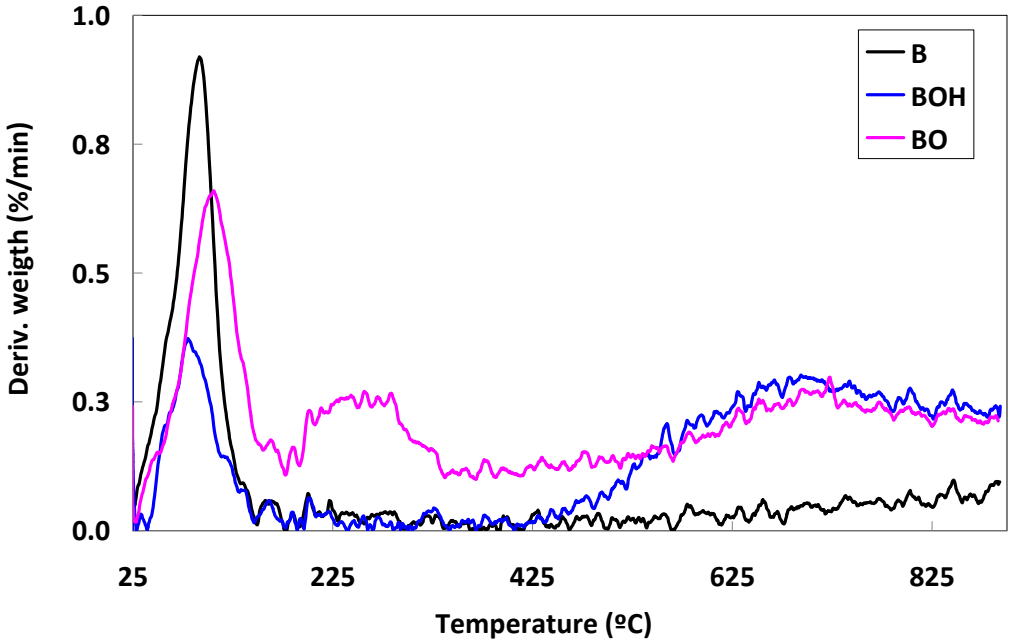

Figure S1. Thermal profiles of the investigated nanoporous carbons.

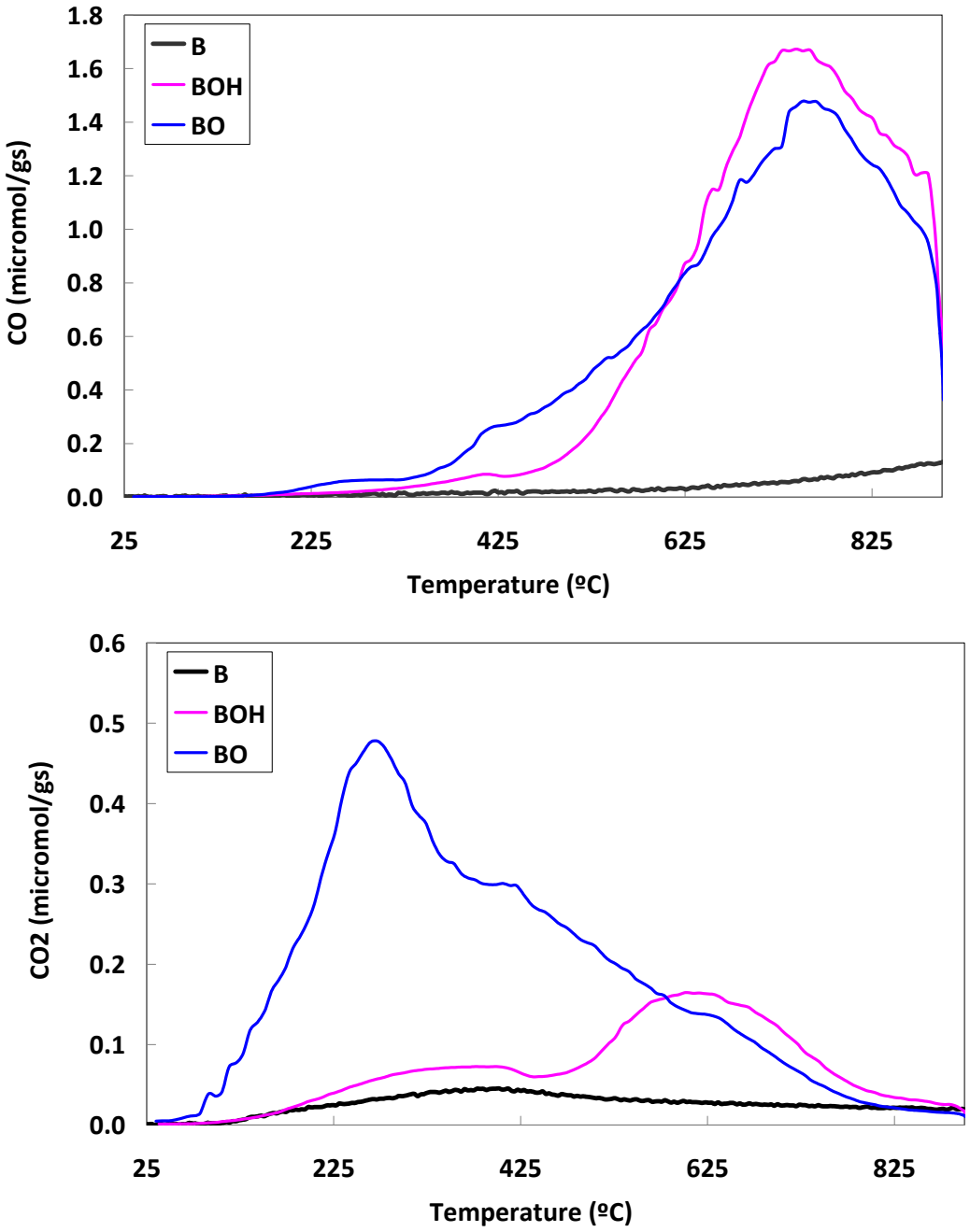

Figure S2. CO (a) and CO_2 (b) profiles of the investigated carbons evaluated by TPD-MS.

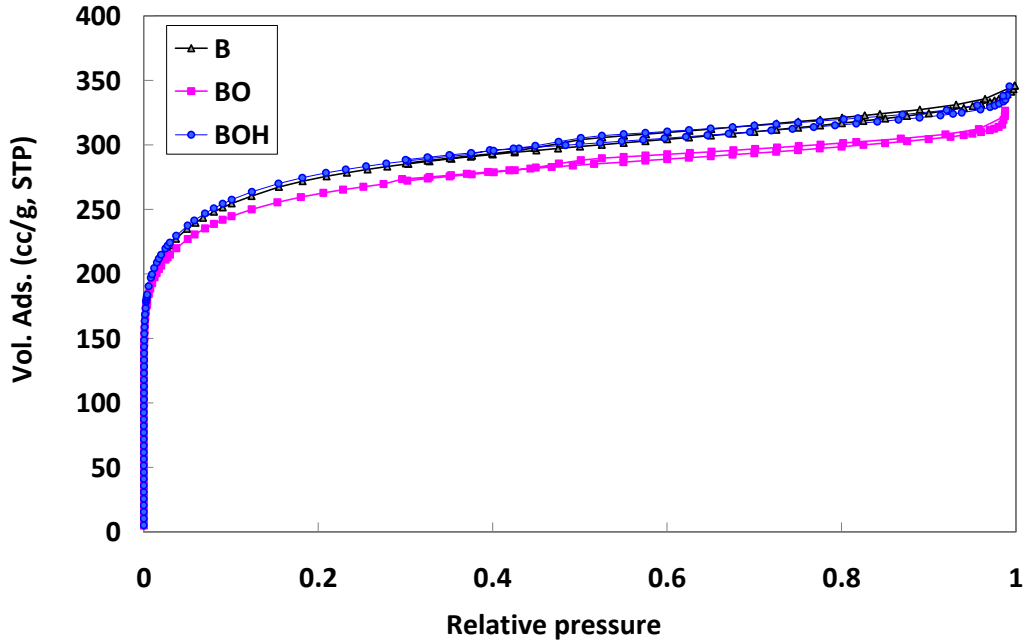

Figure S3. Nitrogen adsorption isotherms at -196 ºC of the investigated nanoporous carbons.

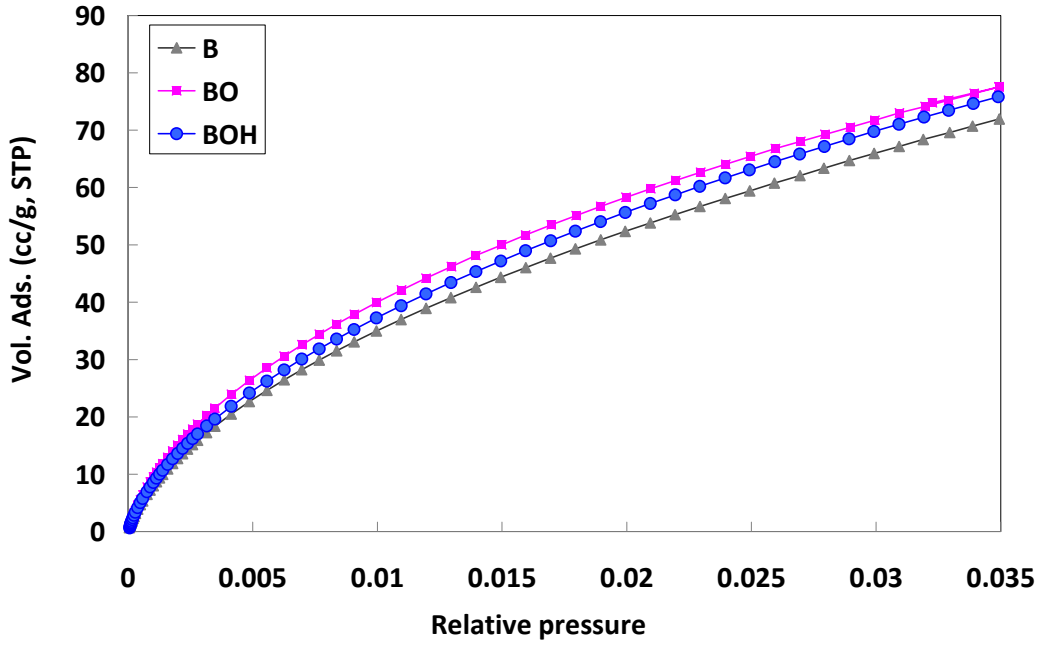

Figure S4. CO_2 adsorption isotherms at -196 ºC of the investigated nanoporous carbons for the evaluation of the narrow microporosity.

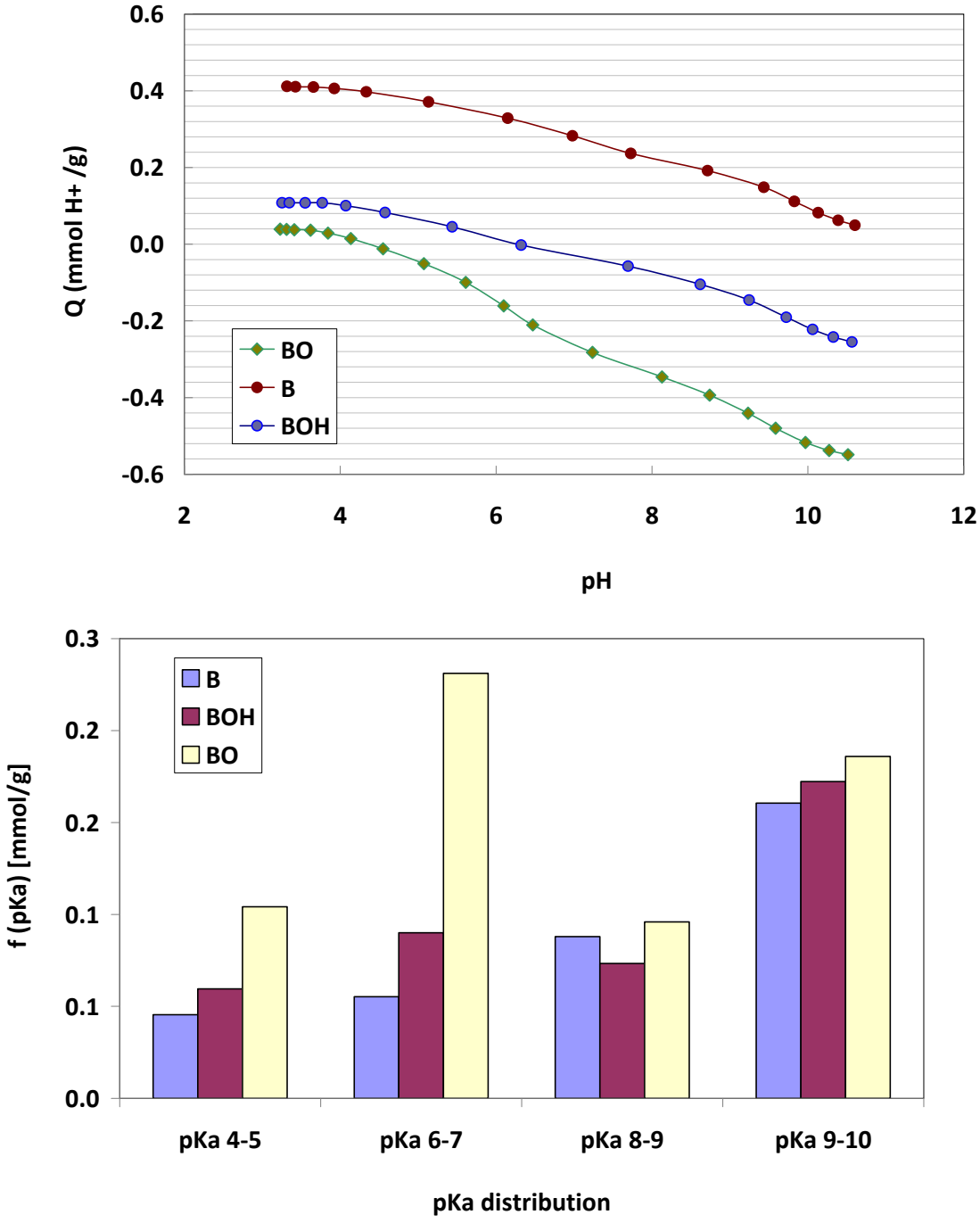

Figure S5. (a) Proton binding curves of the investigated nanoporous carbons for the evaluation of the surface acidity/basicity; (b) distribution of pKa of the surface groups obtained from the proton binding curves.

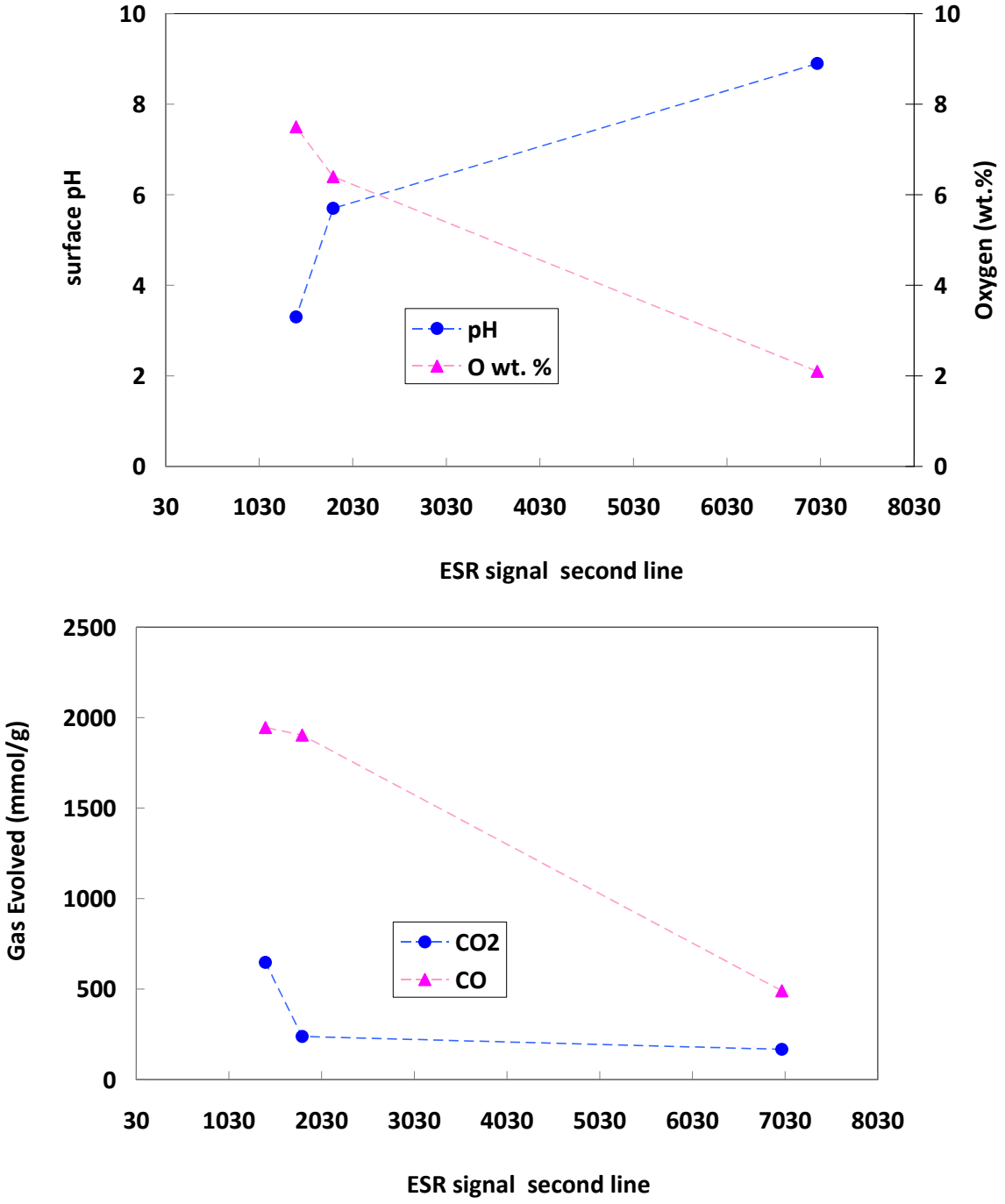

Figure S6. Correlation between the amount of radical species detected by ESR spectroscopy and the surface pH and amount of CO and CO_2-evolved during the TPD-MS analysis.

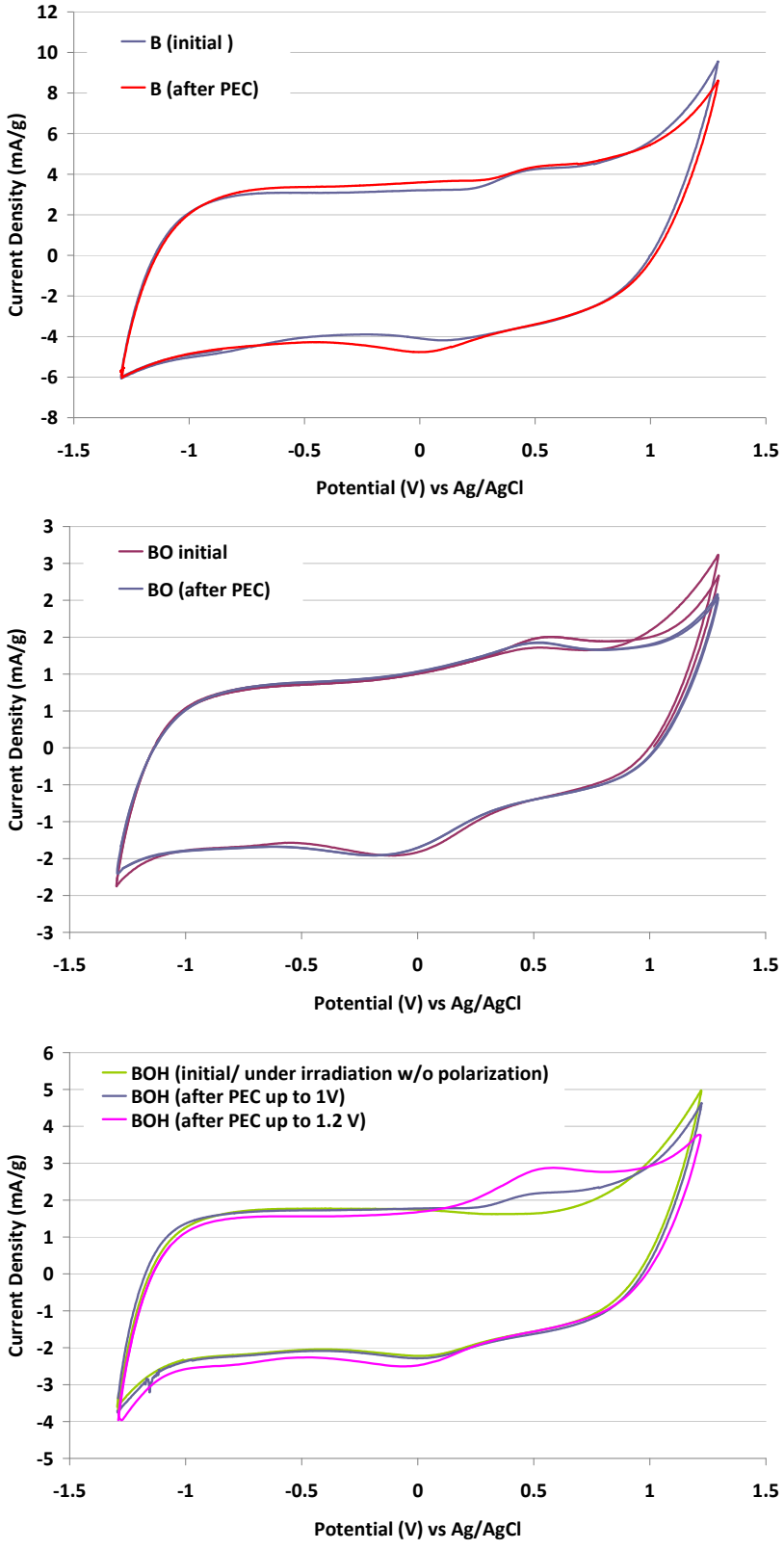

Figure S7. Cyclic voltammograms of B and BOH nanoporous carbon electrodes before and after being submitted to illumination and polarization at high bias potential (PEC). The appearance of humps in the voltammograms indicate the incorporation of O-groups (quinone-type) in the carbon electrodes.

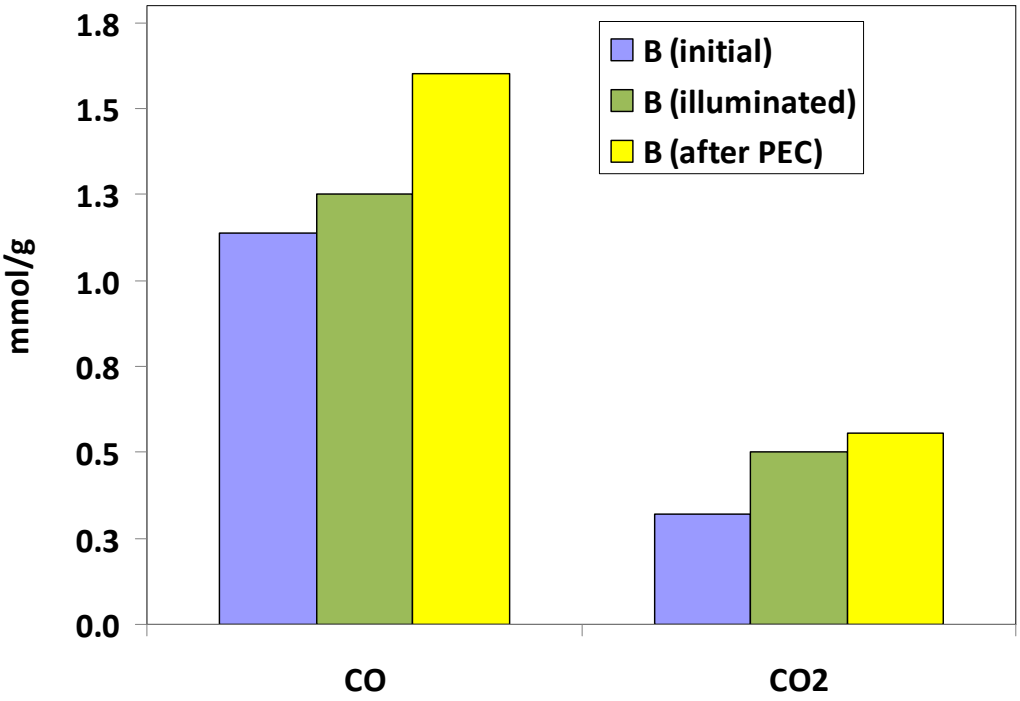

Figure S8. TPD-MS of B electrode before and after being submitted to illumination and polarization at high bias potential.